JOURNAL OF THE KOREAN ASTRONOMICAL SOCIETY
28: 77 ~ 87, 1995

SUNSPOTS AND THEIR ASSOCIATED SOLAR ACTIVITIES
I. PHYSICAL CHARACTERISTICS OF A WHITE LIGHT FLARE

LEE, SANG-WOO AND YUN, HONG SIK
Department of Astronomy, Seoul National University
(Received Mar. 15, 1995;Accepted Apr. 10, 1995)

ABSTRACT

An attempt has been made to analyze time series of Hα, Hβ and Hγ line profiles taken from a 3B/X6.1 flare which occurred on Oct. 27, 1991 in an active region, NOAA 6891. A total of 22 sets of Hα, Hβ and Hγ taken with a low and non−uniform time resolution of 10−40 seconds were scanned by PDS with absolute intensity calibration to derive the physical characteristics of the material in the flare chromosphere. Our results are as follows: (1) The lower Balmer lines observed during the flare activity are broadened by Stark effect. (2) At the peak of the flare activity, the electron temperature of the Balmer line emitting region reaches up to 35000K and its geometrical thickness increases to a scale of $\sim 10^4$km, suggesting that high energy particles penetrate deep into the photospheric level.

Key Words : 3B flare, Balmer lines, physical characteristics

I. INTRODUCTION

Although the white light flare (WLF) was first discovered by Carrington in 1859, its physical characteristics are not well established. The WLF is a very rare event since it is seen in white light on the bright background of the solar surface. Since the first discovery in 1859, only more than 80 events have been reported (Huang *et al.* 1993). The size and life time of the WLF are small, but its peak power can reach 10^{28} ~10^{29} erg/sec, implying that it is a highly energetic phenomenon. The WLF has been considered very important since it provides an excellent means of testing mechanisms of the flare energy transport along with useful diagnostics on the flare process. As can be seen from Svestka's comprehensive reviews on flares (1965, 1972), numerous systematic studies on extracting relevant physical quantities have been made since the early years of flare observations. Quite often, optical line spectra of Balmer series, CaII H and K, and Na D have been utilized to probe the physical conditions of the chromospheric and the upper photospheric flaring site.

In the present study we have examined the shape and temporal behavior of Hα, Hβ and Hγ line spectra of a white light flare (3B/X6.1), which appeared near the disk center in NOAA 6891 on the 27th of October, 1991. The spectra have been taken with the multi−channel spectrograph at Nanjing University. Their spectral shapes are sensitive to the chromospheric conditions and their temporal variations reflect the evolution of dynamics and energetics of the flare activity. Our goal is to gain a physical insight into the overall view of a white light flare quantitatively and qualitatively.

For this purpose we have already looked into the dynamical characteristics of this flare by carefully analyzing the time variations of the red asymmetry of Hα, Hβ and Hγ line profiles during the impulsive phase (Lee *et al.* 1995). From this analysis it is found that (1) the Balmer line emitting region is accelerated downward to 40 km/s for the first 30 s and then is decelerated to 7 km/s for the next 60 s, (2) the turbulent motion within the flare site is found to be as high as 150 km/s, (3) the radial velocity peak precedes the Balmer line peak intensity by 20−40 s, (4) the total energy radiated from these Balmer lines are estimated to be 4.9×10^{29}erg.

The present study focuses only on the physical characteristics of the flare chromosphere by deriving physical quantities such as electron temperature, hydrogen density, geometrical thickness of the Hα, Hβ and Hγ line emitting

region. The observational data and the reduction procedures are briefly described in Section II. In Section III the physical characteristics of the flare are deduced from the line profile analysis and the resulting physical characteristics are presented. Finally, a brief summary and conclusion will be given in Section IV.

II. OBSERVATION and DATA REDUCTION

Figure 1 shows Hα slit jaw image and the position of the slit on the flare kernel. Its field of view is 7×7 arc min. It can be seen that there are one large kernel lying near the sunspot and a few small kernels in the western side of the large kernel. The slit is placed across the larger kernel. The observation was performed with a multi-channel spectrograph attached to the Solar Tower Telescope of Nanjing University. The spectral spatial resolution is estimated to be 3″ and the spectral dispersion is about 1 mm/Å (Huang *et al.* 1993). In order to correct the photospheric contribution to the flare spectra we have taken a set of nearby photospheric spectra on the western side of the large kernel.

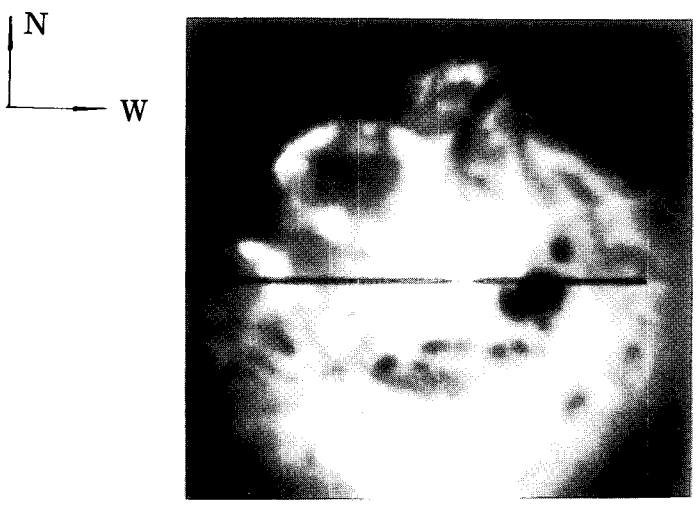

Fig. 1. A Hα slit jaw image of the white light flare at 054040UT of Oct. 27, 1991.

Table 1 shows the time of sequential observations. This flare started at 05:34 UT (Chen *et al.* 1994), but the present observation started at 05:39 UT. Three Balmer line spectral regions have been photographed simultaneously 22 times for the first 10 minutes (05:39:46–05:49:47 UT), where the time interval between exposures has been varied from 10 s to 40 s.

The observed spectra were scanned by PDS to convert photographic density to relative intensity at Purple Mountain Observatory. The spectra have been calibrated to the absolute intensity by choosing several local peak points in the nearby photospheric spectra which is thought to be proportional to the continuum. The relative intensity $R_i(\lambda)$ for each point are read from the spectra and the corresponding absolute intensity $I_i(\lambda)$ is obtained by reading the values off from Table 5A of Labs and Neckel (1970). Then we take the average of the ratios of $I_i(\lambda)$ to $R_i(\lambda)$ for every point to obtain the conversion factor C,

$$C = (1/N) \times \sum I_i(\lambda)/R_i(\lambda), \tag{1}$$

where N is the number of points we selected. The absolute intensity is then obtained by multiplying the relative intensity by C.

Finally, directly observed flare spectrum $I_D(\lambda)$ and nearby photospheric spectrum $I_B(\lambda)$ for each line are then evaluated in absolute intensity unit and the net flare spectrum $I_F(\lambda)$ is obtained by subtracting $I_B(\lambda)$ from I_D (λ).

Table 1. 22 times of exposures.

time sequence no.	UT	time sequence no.	UT
1	053946	12	054257
2	053956	13	054318
3	054011	14	054340
4	054028	15	054356
5	054040	16	054415
6	054056	17	054440
7	054117	18	054515
8	054152	19	054625
9	054204	20	054706
10	054222	21	054816
11	054239	22	054947

The resulting net flare sample profile of Hα line is shown in Figure 2. As can be seen from the figure, their emissivity peaks around the time sequence 5 through 7 for the Hα spectral line.

In order to express the line profile in terms of the wavelength scale, the wavelength calibration is needed. We made the wavelength calibration by choosing two least contaminated metallic lines with a distinct separation whose wavelengths are well established. The wavelengths of our selected metallic lines has been taken from Beckers (1976). This procedure should work well since most of the metallic lines do not show any shift even in large flares (Ding *et al.* 1993).

III. RESULTS

The physical characteristics of the flaring region can be investigated by deriving the physical quantities such as temperature, density and geometrical thickness of the flaring region. In the present work we have focused only on the observed profiles taken at the time sequence of 5 through 7, since they represent the most active, impulsive phase of the flare activity.

In analyzing the spectral data we followed the procedures suggested by Svestka (1965, 1972, 1976), which include checking of line broadening mechanism and estimates of optical thickness, hydrogen number density, electron temperature and departure coefficient from LTE population.

(a) Line Broadening

In this analysis the flare Balmer lines are assumed to come from a slab of optical thickness τ_λ above the quiet photosphere. Hence, the directly observed intensity $I_D(\lambda)$ is given by

$$I_D(\lambda) = I_B(\lambda)\exp(-\tau_\lambda) + S[1 - \exp(-\tau_\lambda)], \tag{2}$$

where the source function S is assumed to be constant. Since the source function varies with optical depth, we have introduced a mean source function defined as

$$S = \frac{\int_0^{\tau_\lambda} S(\tau'_\lambda)\exp[-\tau'_\lambda]\,d\tau'_\lambda}{\int_0^{\tau_\lambda}\exp[-\tau'_\lambda]\,d\tau'_\lambda}. \tag{3}$$

If $\tau_\lambda \ll 1$, S represents reasonably well the actual source function in a slab with an optical thickness τ_λ. Therefore, our analysis works only to the case where the line optical depth meets the condition of $\tau_\lambda \ll 1$.

The wavelength dependence of the source function is assumed to be negligible within a given emission line. In the far wing where $\tau_\lambda \ll 1$, one finds that

$$I_F(\lambda) = I_D(\lambda) - I_B(\lambda) = [S - I_B(\lambda)]\tau_\lambda \tag{4}$$

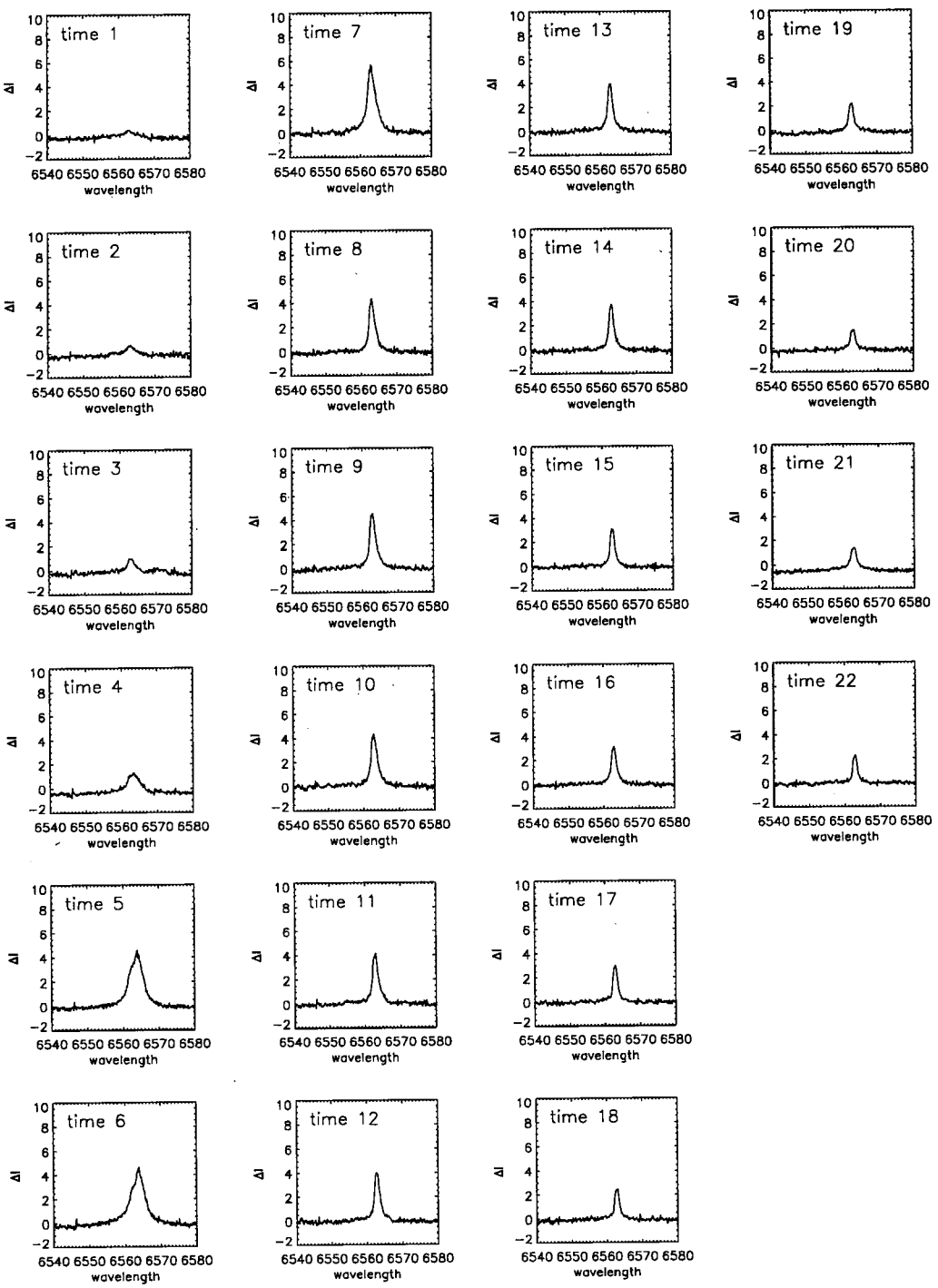

Fig. 2. The net Hα spectra calibrated to the absolute intensity (in unit of 10^6ergs/sec/cm^2/ster/Å).

and

$$\tau_\lambda \propto I_D(\lambda) - I_B(\lambda). \tag{5}$$

Since the net flare spectrum, $I_D(\lambda) - I_B(\lambda)$ can be easily measured from observed profiles, the relationship between $\tau_\lambda(\Delta\lambda)$ and $\Delta\lambda = |\lambda - \lambda_0|$ can be obtained by using equation (5). The functional dependence of τ_λ on $\Delta\lambda$ varies with different line broadening mechanisms. There are two broadening mechanisms that are generally considered for flare emission lines, namely Stark broadening and Doppler broadening, for which τ_λ changes with $\Delta\lambda$ as

$$\tau_\lambda \propto (\Delta\lambda)^{-5/2} \qquad \text{(Stark broadening)} \tag{6}$$

$$\tau_\lambda \propto \exp[-(\Delta\lambda)^m] \qquad \text{(Doppler broadening)}, \tag{7}$$

respectively. We may note that m becomes 2 for the Maxwellian velocity distribution.

If we take a logarithmic form of equation (6) and equation (7), they are written as

$$log(\tau_\lambda) \propto (-5/2) log\Delta\lambda \qquad \text{(Stark broadening)} \tag{8}$$

$$log(\tau_\lambda) \propto -(\Delta\lambda)^m \qquad \text{(Doppler broadening)}. \tag{9}$$

Since τ_λ can be estimated from equation (5), it is possible to examine if the observed Balmer emission lines are broadened by Stark effect or Doppler motions by plotting either $log\Delta I_\lambda$ vs. $log\Delta\lambda$ or $log\Delta I_\lambda$ vs. $\Delta\lambda$ for their line wings.

This procedure is valid only on the line wing portion because the optical depth effect becomes serious as one moves toward the line center. When the deviation from $-5/2$ power law increases toward the line center, the proper wing should be specified and the quantity ΔI_λ at the wavelength $\Delta\lambda$ from the line center should be measured accurately (de la Beaujardiere *et al.* 1992). In the present study, we smoothed the profiles by taking a box average of about 0.2Å twice. Figure 3 shows the smoothed Hα, Hβ and Hγ line profiles. The selected part of the wing is indicated by a symbol $\vdash\dashv$ in the figure. We have measured $\Delta I(\Delta\lambda)$ at specified 10~20 points along the wing of the observed Hα, Hβ and Hγ lines, then plotted $log\Delta I_\lambda$ against $\Delta\lambda$ and $log\Delta\lambda$. The result from Hα line is shown in Figure 4.

As can be seen from the left side of Figure 4, the fitting is almost linear for all profiles, indicating $m \simeq 1$. This implies that the velocity distribution in the flaring region is not Maxwellian if they are Doppler-broadened. The right side of the figure can be used to check out if the lines are broadened by Stark effect. If the fitting is linear and the slope is close to -2.5, then the line wing are broadened by Stark effect. Most of the cases are found to be Stark-broadened. However, there are a few exceptions. For example, the Hα red wing taken at the time sequence 7 and the Hβ red wings taken at the time sequence 6 and 7 clearly deviates from the general trend of the Stark broadening. On the other hand, Hγ profiles are clearly seen to be broadened by Stark effect.

The shape of the red wings of flare emission lines are often affected by the red asymmetry, especially at the peak (time sequence 6 and 7) during the impulsive phase. The fact that Hγ lines do not show any anomaly in our reduced profiles seems to be associated with the depth of line formation. Since Hγ lines are formed at a much deeper layer than Hα or Hβ lines, their profiles are likely to be least influenced by the flare activity than other lines. Accordingly, it is concluded that the Balmer lines observed during the flare are broadened by Stark effect.

(b) Flare Optical Thickness

The next step is to estimate the optical thickness of the flare, which can be done by the procedure suggested by Svestka (1965). Here, we choose an absorption line which overlaps the wing of a Balmer emission line. $\Delta\lambda_A$ is the wavelength distance from a Balmer line center to the center of the selected absorption line and $\Delta\lambda_C$ is that from the Balmer line center to the continuum nearest to the absorption line. Hence the emergent intensities at $\Delta\lambda_A$ and $\Delta\lambda_C$ are expressed as

$$I(\Delta\lambda_A) = I_0(\Delta\lambda_A)\exp[-\tau(\Delta\lambda_A)] + S\{1 - \exp[-\tau(\Delta\lambda_A)]\} \tag{10}$$

$$I(\Delta\lambda_C) = I_0(\Delta\lambda_C)\exp[-\tau(\Delta\lambda_C)] + S\{1 - \exp[-\tau(\Delta\lambda_C)]\}. \tag{11}$$

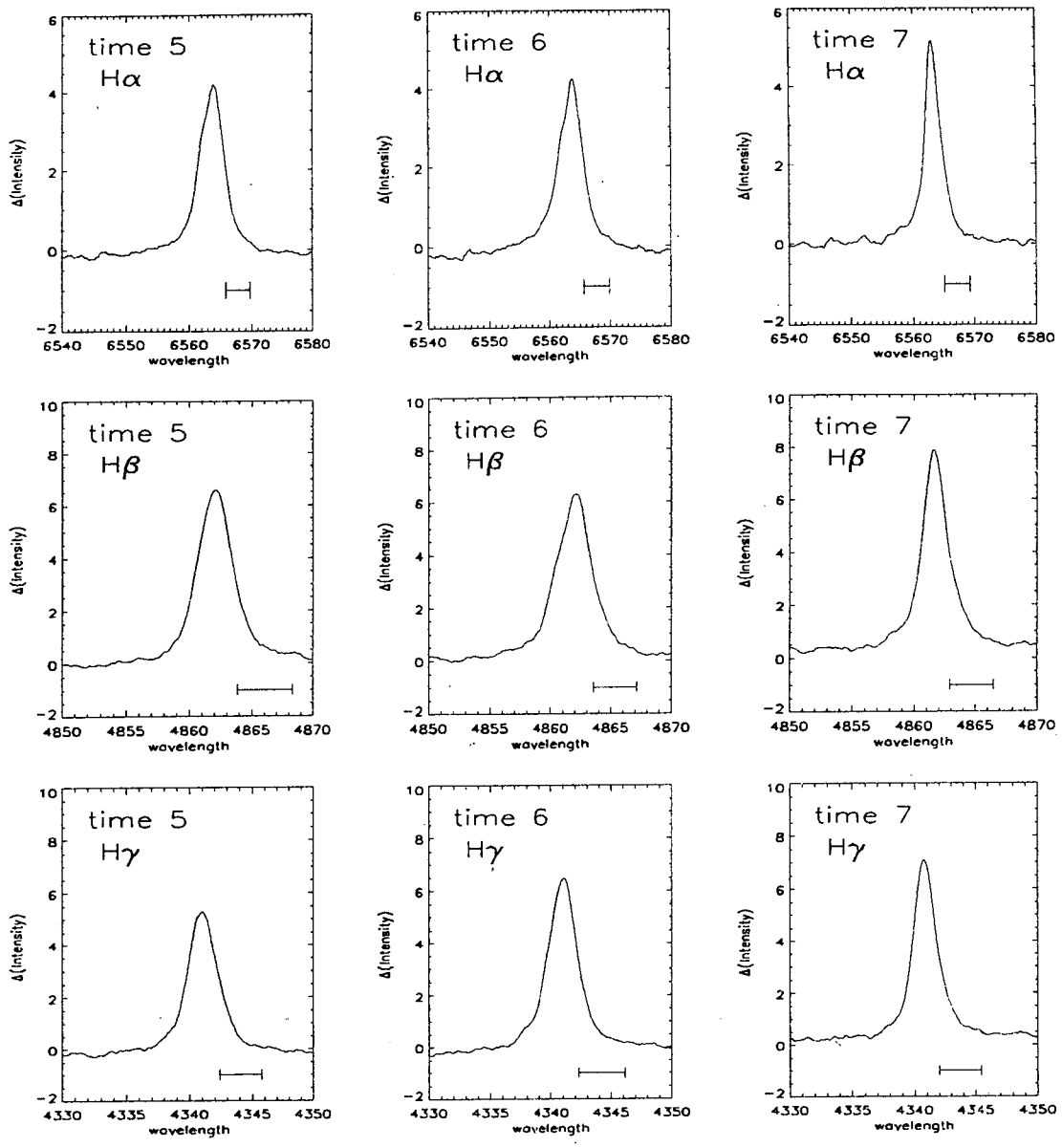

Fig. 3. The smoothed Hα, Hβ and Hγ profiles.

If $|\Delta\lambda_A - \Delta\lambda_C|$ is sufficiently small and far wings are considered, it can be said that $\tau(\Delta\lambda_A) \approx \tau(\Delta\lambda_C)$. So the optical thickness $\tau(\Delta\lambda_A)$ at $\Delta\lambda_A$ can be estimated from

$$\exp[-\tau(\Delta\lambda_A)] = \frac{I_D(\Delta\lambda_C) - I_D(\Delta\lambda_A)}{I_B(\Delta\lambda_C) - I_B(\Delta\lambda_A)}. \tag{12}$$

Therefore, once we measure the line depth of an absorption line adjacent to the Balmer line for both of the flare and the quiet photosphere, then the optical thickness is easily estimated from equation (12). In the case of Hα, only one absorption line, FeI 6569.22 has been used because of the cleanness in the observed profiles. For the cases of the Hβ and Hγ, two absorption lines (FeI 4859.75 and TiII 4865.64 for Hβ and FeI 4337.06 and TiII 4337.92 for Hγ) have been used because of the complexity in the observed wing profiles. The resulting optical thickness of the Hα emitting region at the impulsive phase are listed in Table 2.

The estimated optical thickness is bound to be inaccurate, since the line depths cannot be measured accurately.

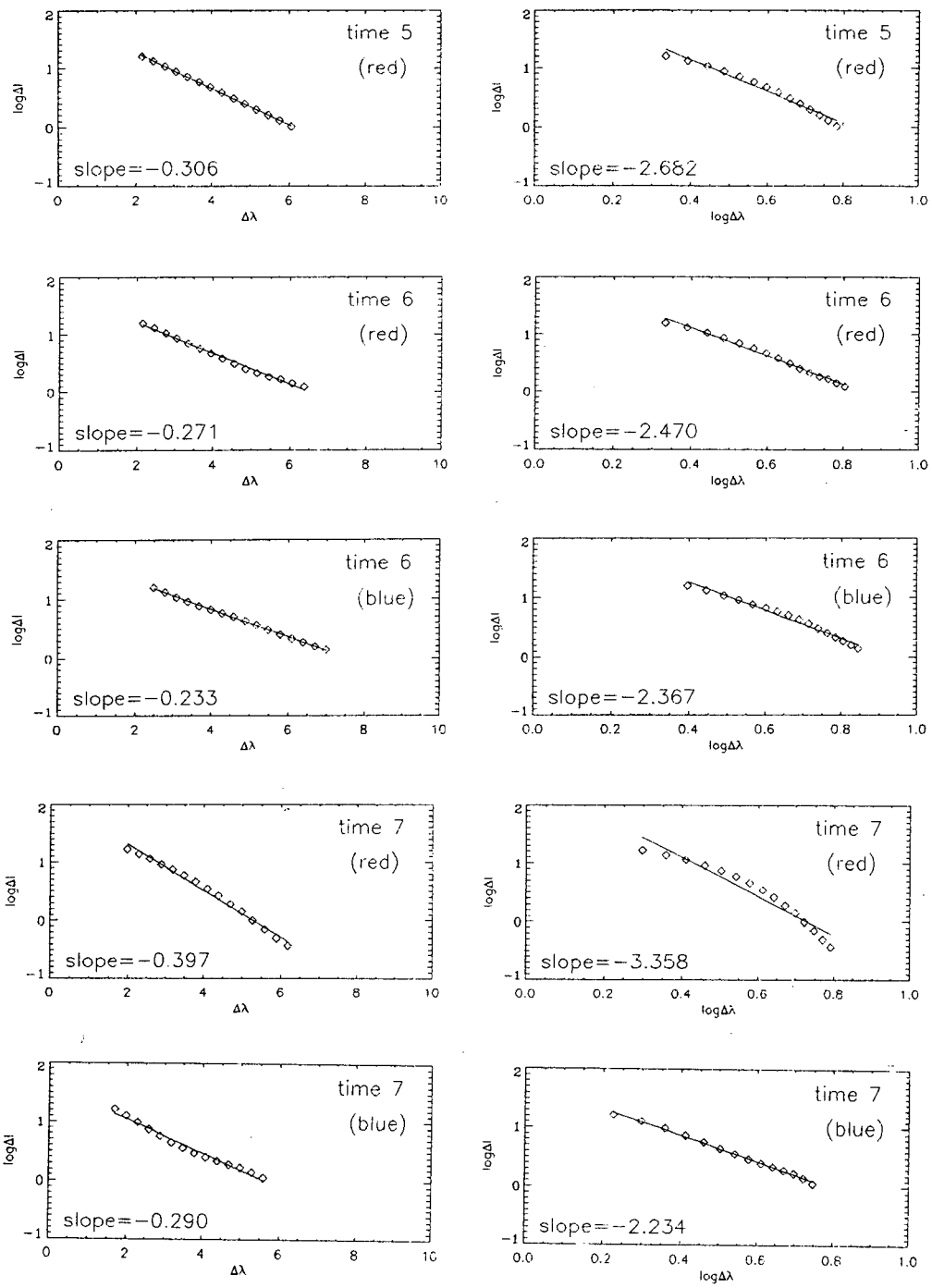

Fig. 4. Checks on broadening mechanism for Hα line. The left column is $log\Delta I_\lambda$ vs. $\Delta\lambda$ plot, and the right column is $log\Delta I_\lambda$ vs. $log\Delta\lambda$ plot. The slope is also included.

The major difficulty is to correct the noise present in the line spectra under consideration. The intensity of the continuum nearest to the selected absorption line and that of its center should be also measured within a reasonable accuracy to obtain the line depth. However, the identification of the continuum level is difficult to make because of the noise present in the far wings of the line. The noise in the spectra can be reduced somewhat by smoothing, but it also removes the important information on the line center. For this reason, in the present analysis the smoothing has been made with a box average of only 5 pixels (0.1Å).

Table 2. The estimated optical thickness values of the Hα emitting region.

time sequence	$\tau(\Delta\lambda)$-measured	$\tau(\Delta\lambda)$-corrected
5	0.218	0.144
6	0.391	0.368
7	0.331	0.265

Table 3. The estimated N_2 values at the time sequence 7 (10^{16}cm^{-2}).

T_e	Hα	H$\beta-1$	H$\beta-2$	H$\gamma-1$	H$\gamma-2$	mean value
8000	2.72	0.96	1.90	3.22	1.50	2.17
10000	2.86	1.00	1.98	3.36	1.57	2.27

(c) Column Density in the Second Level of Hydrogen

In view of the fact that the Balmer emission lines are broadened by Stark effect, equation (13) valid for the Stark broadened lines has been used to obtain N_2, column density of hydrogen in the second level,

$$\tau(\Delta\lambda) = 321 C_u k n_e \Delta\lambda^{-5/2}(1 + R\Delta\lambda^{1/2})N_2 \tag{13}$$

with

$$R = 4.6\frac{Y(u)}{T_e^{1/2}}\left[log\left(\frac{4\times10^6 T_e}{u^2 n_e^{1/2}}\right) - 0.125\right] \times \frac{u^5 + l^5}{u^2 l^2 (u^2 - l^2)^{1/2}} \tag{14}$$

and $C_u = 3.13 \times 10^{-16}$ and $Y(u) = 1.5$ for Hα, $C_u = 0.88 \times 10^{-16}$ and $Y(u) = 1.12$ for Hβ and $C_u = 0.44 \times 10^{-16}$ and $Y(u) = 1.06$ for Hγ (Gray 1976), where u refers to the upper level and l the lower level. In order to estimate N_2, values of electron density, n_e and electron temperature, T_e are needed together with the value of $\tau(\Delta\lambda)$.

The electron density is often obtained from the halfwidth of high Balmer lines (Svestka 1965, 1972, 1976). Since high Balmer line data are not available in the present work, we were not able to obtain the electron density. Electron densities of flares are known to range from 10^{12} to 10^{13}cm^{-3}. Recently, Neidig *et al.* (1993) claimed that n_e should be $n_e > 10^{13}\text{cm}^{-3}$ in order to account for the observed Balmer line spectra of large flares. In the present study we have adopted $n_e = 3 \times 10^{13}\text{cm}^{-3}$ as a representative value for the impulsive phase (Svestka 1976), and 8000K and 10000K have been taken as a set of trial values for electron temperature.

With the use of equation (13) and equation (14), N_2 has been estimated at the time sequence 5 through 7, where we have used the values of the estimated $\tau(\Delta\lambda)$ in Table 2. The resulting values of N_2 at the time sequence 7 are listed in Table 3, where we note that they differ from each other. Ideally, for a given temperature all of the estimated N_2 values should be identical. The discrepancy appears to be attributed to the noise present in the observed line profiles and the inaccuracy in measurements of the line depth.

Hence, we took an average of the five N_2 values, weighting 2 for the estimates made by Hα and 1 for the ones made by Hβ and Hγ. This uneven weight given to the lower Balmer lines is based on the quality of the observed line profiles and the accuracy of the estimates of N_2. With the use of the new N_2, we have recalculated the optical thickness $\tau(\Delta\lambda)$ of the Balmer line emittng region by using equatin (13).The corrected $\tau(\Delta\lambda)$ values are listed in the last column of Table 2.

(d) Electron Temperature

In the hydrogen lines the electron temperature can be estimated from the population at different quantum states. With the use of equation (4) the line source function S can be written as

$$S = [I_D(\Delta\lambda) - I_B(\Delta\lambda)]/\tau(\Delta\lambda) + I_B(\Delta\lambda). \tag{15}$$

The Balmer line source function S is related to the ratio of the density of hydrogen atoms in the sth and the second quantum states,

$$n_s/n_2 = S_\lambda(s^2/4)(\lambda^5/2hc^2). \tag{16}$$

The population ratio between the two quantum states is represented as

$$n_s/n_i = (b_s/b_i)(s/i)^2 \exp(-hc/k\lambda_{si}T_e) \tag{17}$$

and

$$n_s/n_i = (s/i)^2 \exp[-hc/k\lambda_{si}T_\alpha(s,i))], \tag{18}$$

where the b_i represents the deviation in level populations from LTE at a given T_e and the λ_{si} is the wavelength corresponding to the two level (s,i) transition with s=3,4,5 and i=2,3,4 in our case. As noted from equation (18), the electron temperature T_e is associated with the excitation temperature T_α. The excitation temperatures $T_\alpha(s,i)$ between levels s and i for every s and i can be computed by substituting equation (16) into equation (18). Since the higher levels are populated predominantly by collisions while the lower levels by radiation, T_α should be lower than T_e. As s and i increase, $T_\alpha(s,i)$ gets closer to T_e because the departure coefficient b_s(or b_i) converges to 1.0. Hence, the maximum value of $T_\alpha(s,i)$ may be regarded as the electron temperature T_e as a first approximation.

Since we deal with a hydrogen atom of only 5 levels, there must exist some discrepancy between T_α and T_e. However, the discrepancy should be small in view of the fact that b_5 is generally very close to 1.0 (Neidig *et al.* 1993; Svestka 1965). The excitation temperatures deduced from Hα, Hβ and Hγ lines at the time sequence 6 are presented in Table 4, where the inferred electron temperature is also included. With the use of the inferred electron temperature the departure coefficients $b_s(s = 3,4,5)$ have been determined by equation (17), where we assumed $b_5 = 1$. Table 5 lists the computed departure coefficients b_s at the 4 excited states.

Table 4. Estimation of electron temperature at the time sequence 6.

j \ i	2	3	4	T_e
3	6850	——	——	
4	6740	6450	——	~35000
5	7340	8540	28380	

Table 5. The estimated departure coefficients.

time sequence	b_2	b_3	b_4	b_5
5	14.19	2.40	1.02	1.00
6	35.71	2.71	1.04	1.00
7	9.90	2.22	1.03	1.00

(e) Hydrogen Number Density

With the knowledge of n_e and b_s the average number density n_s at an excited level s can be determined from the combined Boltzmann-Saha equation,

$$n_s = 4.15 \times 10^{-16} b_s s^2 n_e^2 T_e^{-3/2} \exp(\chi_s/kT_e) \qquad (s \geq 2), \tag{19}$$

where χ_s is the ionization potential from the sth quantum level. The computed n_s are tabulated in Table 6.

Since the newly estimated T_e in Table 4 is now available, N_2 can be recalculated by using equation (13) and equation (14). The recomputed N_2 values are listed in Table 7. As can be seen from the table, N_2 is found to be of the order of 10^{16}cm^{-2}. Since the column density N_2 is given by

$$N_2 = n_2 \cdot \Delta z, \tag{20}$$

Table 6. The estimated hydrogen number density (cm^{-3}).

time sequence	n_2	n_3	n_4	n_5
5	3.90×10^7	5.48×10^6	2.92×10^6	3.81×10^6
6	2.51×10^7	2.29×10^6	1.26×10^6	1.71×10^6
7	1.49×10^8	1.57×10^7	7.51×10^6	8.84×10^6

Table 7. The new estimated N_2 values ($10^{16}cm^{-2}$).

time sequence	Hα	H$\beta-1$	H$\beta-2$	H$\gamma-1$	H$\gamma-2$	mean value
5	1.04	0.99	0.99	1.04	1.03	1.02
6	3.00	2.78	2.79	2.96	2.91	2.91
7	2.44	2.37	2.39	2.43	2.42	2.42

the linear thickness of the flare along the line of sight can be estimated. The estimated geometrical thickness is estimated to be 11590km at the time sequence 6, which shows that the flaring region can be grown to a scale of $\sim 10^4$km at the peak of the flare activity.

IV. SUMMARY AND CONCLUSION

We have analyzed time series of the lower three Balmer line profiles which had been taken from a 3B white light flare appeared in NOAA Region 6891 on October 27, 1991. Each set of the spectra was taken simultaneously for the first 10 minutes of the flare event with a low and uneven time resolution of 10–40s. The observations have been made by the multi-channel spectrograph attached to Solar Tower Telescope of Nanjing University. A total of 22 sets of Hα, Hβ and Hγ were scanned by PDS to make their absolute intensity calibration.

The physical characteristics of the flare have been examined by deriving physical quantities such as electron temperature, hydrogen density and geometrical thickness. The important findings emerging from the present investigation are summarized as follows:

(1) The Balmer emission lines observed in this flare are found to be broadened by Stark effect.

(2) At the peak of the flare activity the electron temperature of the flaring region reaches up to ~35000K.

(3) The column density of the hydrogen atom in the first excited state amounts to $3 \times 10^{16}cm^{-2}$.

(4) The geometrical thickness of the Balmer line emitting region has grown to a scale of $\sim 10^4$km, suggesting that the ejected high energy particles have penetrated deep into the photospheric level.

These conclusions have been derived mainly from the lower Balmer line spectra observed during 10 minutes around the flare maximum. However, they are certainly hampered by the incompleteness of data. The following aspect should be considered for improvement. To probe the physical conditions in detail, a care should be taken in selecting spectral lines as well as in including all the important lines. In the case of Balmer lines, both of the lower and higher Balmer lines should be observed simultaneously. High Balmer lines allow us to deduce the electron density either by the half–width method or by Inglis–Teller formula.

ACKNOWLEDGEMENT

We are very grateful to Drs. J. Hu and C. Fang for providing us with this observed white light flare spectra. We also wish to thank Dr. J. W. Lee for his valuable comments. The present studies were supported by the Basic Science Research Institute Program, Ministry of Education 1994 (BSRI–94–5408).

REFERENCES

Beckers, J. M., Bridges, C. A. & Gilliam, L. B. 1976, *A High Resolution Spectal Atlas of the Solar Irradiance from 380 to 700 Nanometers*, Air Force Geophysics Laboratory.

Chen, J., Huang, Y. & Liu, Z. 1994, *Solar Phys.*, **150**, 179.
de la Beaujardi re, J. -F., Kiplinger, A. L. & Canfield, R. C. 1992 *Ap. J.*, **401**, 761.
Ding, M., Fang, C. & Okamoto, T. 1993, *Chin. Astron. Astrophys.*, **17/4**, 413.
Gray, D. F., 1976, *The Observation and Analysis of Stellar Photospheres*, John Wiley and Son Inc., p247.
Huang, Z., Ma, L., Fang, C. & Hu, J. 1993, *Chin. Astron. Astrophys.*, **17/3**, 291.
Labs, D. & Neckel, H. 1970, *Solar Phys.*, **15**, 79.
Lee, S. W., Yun, H. S., Hu, J., Fang, C. & Wang, J. L. 1995, *Solar Phys.*, submitted.
Neidig, D. F., Kiplinger, A. L., Cohl, H. S. & Wiborg, P. H. 1993, *Ap.J.*, **406**, 306.
Svestka, Z. 1965, *Adv. Astron. Astrophys.*, **3**, 119.
Svestka, Z. 1972, *A. R. A. A.*, **10**, 1.
Svestka, Z. 1976, *Solar Flares*, D. Reidel Publ. Co., Dordrecht, Holland.